EARTH SCIENCES
RESEARCH JOURNAL
Earth Sci. Res. J. Vol. 26, No. 4 (December, 2022): 321 - 333

UNIVERSIDAD NACIONAL DE COLOMBIA

ORE GEOLOGY

Investigation of the spatial distribution of porphyry copper deposits using fractal and fry analysis methods in Dehaj Area, Kerman: Implications for exploration

Narges Habibkhah[1*], Hossein Hasani[1], Abbas Maghsoudi[1], Mehdi Honarmand[2]
Amirkabir University of Technology, Iran
University of Advanced Technology, Iran
*Corresponding author: n.habibkhah@aut.ac.ir

ABSTRACT

Known to be triggered and controlled by tectonic systems, magmatism plays a significant role in the deposition and emplacement of hydrothermal mineral systems. It is, therefore, of paramount importance to recognize the tectonic processes that are genetically associated with hydrothermal mineral systems. This study seeks to address this research gap by recognizing the main tectonic processes that have controlled the distribution of porphyry copper (Cu) deposits in Dehaj Area on the Urmia-Dokhtar magmatic belt, central Iran. For this purpose, spatial associations of 31 known porphyry Copper deposits, faults, and fractures were evaluated by multiple numerical techniques including fry, fractal, (box-counting and radial-density methods), and distance-distribution analyses to investigate structural controls of the porphyry Copper mineralization. Results of the fry analysis revealed three mineralization trends, namely NS, NE, and NW, clearly following the existing fault systems in the area. Application of the fractal method demonstrated that structural controls on mineralization have operated on two different scales, regional and local scales. Distance-Distribution analysis was further used to spatially correlate known porphyry Copper deposits to fault traces, supplementing the results of fry and fractal analyses by quantitative measurements. Compiling the results of these three methods, it was shown that NW-trending faults have plausibly controlled the magmatism on a regional scale. On a local scale, however, NE- and N-trending faults have probably acted to control the channelling and emplacement of mineral-bearing fluids.

Keywords: structural controls; porphyry Cu deposits; fry; fractal; distance-distribution analysis; Urmia-Dokhtar magmatic belt; Iran.

Investigación de la distribución espacial de depósitos de pórfido cuprífero a través del método de Fry y métodos fractales en el área de Dehaj, Kerman: Implicaciones para la exploración

RESUMEN

El magmatismo, conocido por ser desencadenado y controlado por sistemas tectónicos, juega un rol importante en la deposición y emplazamiento de sistemas minerales hidrotermales. Es fundamental, entonces, reconocer los procesos tectónicos que están genéticamente asociados con los sistemas minerales hidrotermales. Este trabajo está enfocado en esta falta de datos al establecer los principales procesos tectónicos que han controlado la distribución de depósitos de pórfido cuprífero en el área de Dehaj, en el cinturón magmático de Urmia-Dokhtar, en el centro de Irán. Con este propósito se evaluaron las asociaciones espaciales, las fallas y las fracturas de 31 depósitos conocidos de pórfido cuprífero a través de técnicas numéricas que incluyen el método de Fry (extrapolación), fractal (método de conteo de cajas y de densidad radial), y análisis de distribución de distancia para investigar los controles estructurales de la mineralización del pórfido cuprífero. Los resultados de los análisis de extrapolación revelaron tres tendencias en la mineralización, NS, NE, y NW, lo que claramente coincide con los sistemas de fallas en el área. La aplicación del método fractal demostró que los controles estructurales en la mineralización han operado a escala regional y a escala local. El análisis de distribución de distancias fue usado luego para relacionar los depósitos de pórfido cuprífero con las trazas de las fallas y complementar así los resultados de las medidas cuantitativas del método de Fry y de los análisis fractales. La compilación de los resultados de estos tres métodos muestra que las fallas con tendencia NW problablemente han controlado el magmatismo a escala regional. A escala local, sin embargo, las fallas con tendencia NE y N han controlado la canalización y el emplazamiento de fluidos con minerales.

Palabras clave: Controles estructurales; depósitos de pórfido cuprífero; método de Fry; fractal; análisis de distribución de distancias; cinturón de Urmia-Dokhtar; Irán

Manuscript Received: 09/10/2019
Accepted for Publication: 11/01/2023

How to cite this item:
Habibkhah, N., Hasani, H., Maghsoudi, A., & Honarmand, M. (2022). Investigation of spatial distribution of porphyry copper deposits using fractal and fry analysis methods in Dehaj Area, Kerman: Implications for exploration. *Earth Sciences Research Journal, 26*(4), 321-333. https://doi.org/10.15446/esrj.v26n4.82748

ISSN 1794-6190 e-ISSN 2339-3459
https://doi.org/10.15446/esrj.v26n4.82748

1. Introduction

An array of hydrothermal mineral deposits, including porphyry Cu deposits (Sillitoe, 1972; Sillitoe, 2010) are conventionally thought to be controlled structurally (Pirajno, 2012). That is, structural features, ranging from faults to fractures, act as major corridors for migration of mineral-bearing fluids (Pirajno, 2012; Parsa and Maghsoudi, 2018). Although distribution and emplacement of hydrothermal mineral systems are inextricably linked to fault systems, not all fault systems are associated with this type of mineralization (cf. Faulkner *et al*., 2010). It is, therefore, crucial to answer the question of how is the distribution of hydrothermal mineral deposits associated with faults? The answer to this question is important in that the fault systems that exhibit spatial and genetic link with mineral deposits can serve as exploration criteria for the delineation of exploration targets (e.g., Carranza, 2009; Carranza and Sadeghi, 2014; Adib *et al*., 2017a; Adib *et al*., 2017b; Parsa *et al*., 2018a; Parsa and Maghsoudi, 2018).

Located in the southern part of Urmia-Dokhtar magmatic belt (Fig. 1), Dahej Area is dominated by magmatic sequences. In this area, the magmatism is known to have been commenced by the deposition of acidic-to-intermediate extrusions in Eocene, and then lasted till Quaternary when basaltic outcrops have been emplaced. The acidic-to-intermediate plutonic sequences have been then intruded by shallow Oligocene-Miocene dioritic and granitic intrusions. Not only did these intrusions trigger the development of extensive alteration zones, but they hosted a number of metallic deposits (Feizi *et al*., 2017a) such as porphyry Cu mineralization in the area (Feizi *et al*., 2017b); that is, these intrusions are spatially and temporally associated with mineralization (Zarasvandi *et al*., 2016). Although many studies have been conducted on these deposits (e.g., Khoie *et al*., 1999; Bazin and Hubner, 1969; Dehghani, 2000; Zarasvandi, 2004; Mehrabi *et al*., 2005; Zarasvandi *et al*., 2016), their spatial link with structural features remains unanswered. Accordingly, the present research aimed at tackling the foregoing caveat gap through spatial and numerical techniques.

Faults, fractures, shear zones, and various spatial stresses tend to concentrate the magma and trigger its movement through shallow zones of the crust, indicating their crucial role in the distribution of magmatic fluids (Ryan and Dewey, 1990). Therefore, investigation of the geometry of the fault mechanisms associated with porphyry Cu orebodies can lead to very significant insights into the choice of proper locations for exploring porphyry bodies (Walker, 2006). Different analyses have been conducted to assess spatial distribution of mineral deposits; however, the most profound methods of analysis are seemingly the fractal (Mandelbrot, 1983) and fry analyses (Fry, 1979), which we were used in this study. In addition, there are myriad numerical techniques available for assessing spatial association of faults systems with mineralization. These include, for example, the t-student spatial statistics (Zuo *et al*., 2009; Xiao *et al*., 2012; Zuo and Wang, 2015; Parsa *et al*., 2017a; Parsa *et al*., 2017b; Parsa *et al*., 2017c), success-rate curves (Agterberg and Bonham-Carter, 2005; Mirzababaei, 2016; Parsa *et al*., 2016a; Parsa *et al*., 2016b), distance-distribution analysis, and receiver operating characteristics (ROC) curves (Berman, 1977; Berman, 1986; Haddad-Martim *et al*., 2017; Parsa *et al*., 2018b). Among others, ROC curves provide for superior robustness and visual assessment of the relationship between structures and mineral deposits (cf. Carranza, 2009; Agterberg, 2013; Lisitsin, 2015; Haddad-Martim *et al*., 2017; Parsa *et al*., 2018a; Ramezanali *et al*., 2019). In Iran, ROC analysis has been used to investigate spatial distribution of chromite (Yaghoubpour and Hassan Nezhad., 2006), Pb-Zn (Hassannejad *et al*., 2001), iron (Najafi *et al*., 2010) and Cu deposits (Tanhaei *et al*., 2010, Zarasvandi *et al*., 2016). In this paper, two principal objectives were followed: (1) to investigate structural elements and (2) to identify relationship between these structures and mineralization. In this regard, fry (Fry, 1979), fractal (Mandelbrot, 1983) and distance-distribution (Berman, 1977, 1978) analyses were utilized to investigate structural controllers. As a result of these analyses, we could develop a suitable method for determining the main directions of dispersion of deposits with respect to linear structures. A combination of these methods has rarely been devised to investigate the spatial pattern of porphyry Cu deposits, with the results contributing to delineation of prospective areas for exploration activities.

2. Geological setting

Study area is located in the southwest of Central Iran, covering parts of the Sanandaj – Sirjan Zone and Urmia-Dokhtar magmatic belt (Dimitrijevic, 1973).

2.1. Stratigraphy

On the surface, the study area is covered by sedimentary, igneous, and metamorphic rock units that have been dated back to Palaeozoicto the present age, generally trending along a NW – SE direction. Dated back to Palaeozoic, the oldest deposits constitute the bedrock and are, in most cases, metamorphized. Exposed in parts of the Sanandaj – Sirjan Zone and Central Iran, these rocks are separated from the Sahebabad – Marvast Desert Embayment by the Marvast – Herat Fault which strikes along an NNW – SSE direction. This fault has remained active during the quaternary, leading to a drop down of the eastern wall with respect to the western wall. Metamorphized and non-metamorphized Permian rocks represent the youngest units of Palaeozoicage in this area. The rock units in this area have been subjected to two phases of metamorphism; one during the Triassic and another one during the Upper Jurassic. Various zones are separated from one another by faults in the NW-SE direction, some of which are further inclined toward an E-W direction (Soheili, 1981; khakzad and Jaafari, 2002).

An Upper Cretaceous colouredmélange zone is developed in the form of a narrow stripe with a width of about 3 -17 km and a length of about 125 km along the general trend of the region. This zone is mainly composed of basalt, split rock, green tuff, tuffy sandstone, ultra-basaltic rocks, limestone, and radiolaria, which are exposed in the tectonic zone. Adjacent to this zone, multiple faults are developed along a NW – SE direction, which together comprise a part of the Naein – Baft Main Fault. In between this zone and the Marvast – Herat Fault, there is an extensive embayment in the form of a graben, which includes the Sahebabad – Marvast Desert, that is itself a part of the greater embayment of Gavkhooni – Sirjan and hosts quaternary deposits. Besides the colouredmélange unit, there are Eocene volcanic rocks, indicating that the mentioned tectonic zone has been partly active in Eocene as well (Soheili, 1981).

The Urmia – Dokhtar Zone includes the highlands in the west, centre, and north of the mapped area. In this zone, limestones comprise the oldest rock unit, while the Upper Cretaceous densely folded flysches are ended up located at the centreof an anticline in the east. Due to the continental drift in Eocene, large amounts of lava and volcanoclastic rocks with basic and alkaline composition were emitted through deep paleo-fractures, with the Eocene sedimentary deposits formed at the same time. Following the Eocene, the compressive force melted the continental crust, developing intrusive rocks with the general composition of granodioritic and monzonitic quartz that cut through the Eocene rocks. During the Neogene, another round of extensive volcanic activities occurred with a moderate to acidic composition, and associated lava and volcanoclastic rocks covered the older rock units. An example of such volcanic activities occurred at Mozahem Volcano in the NE of Shahr-e-Babak (Soheili, 1981).

In Quaternary, a semi-deep mass of porphyry and dacitic micro-granodioritic rocks cut through the older strata, forming some light-coloured uplifts in mountainous areas. Intrusion of these semi-deep rock units and associated metamorphism have contributed to the formation of porphyry Cu orebodies and veins and minor accumulations of lead and zinc in this area. In the NW corner of the mapped area, the Upper Cretaceous is represented by highly folded and partly metamorphized flysches, and a NW-SE-trending syncline is seen in this area. The syncline is followed by Kerman Conglomerates and hosts some Middle Eocene lavas in the middle. The Anar Embayment is seen as a graben in between the Badbakhtkooh and mountain ranges in the central part of the mapped area, encapsulating the quaternary deposits. Rock bodies of granite, andesite, granodiorite, and diorite are dispersed as intrusions into the space between the main rock units of region (Fig. 2) (Soheili, 1981; Mirzababaei, 2016).

A total of 130 metallic and non-metallic mineralization occurrences are reported in this study area, including metallic reserves of Cu, Cu- gold, iron, and lead-zinc and non-metallic reserves of bentonite, stone, gypsum- anhydrite, industrial, phosphate, kaolin, soils, perlith, silica and pozzolan.

2.2. Structural geology

In addition to the Marvast – Herat Fault, there are three other faults in the mapped area, namely Anar, Shahr-e-Babak, and Rafsanjan faults. A major part of Anar Fault is extended beyond this area, but its southern end passes through the west of Anar City. Shahr-e-Babak is a dextral strike-slip fault with a length of 235 km that is developed along a NW-SE trend. Seemingly, Anar and Rafsanjan faults intersect on the west of the area (Soheili, 1981; Zarasvandi *et al*., 2016).

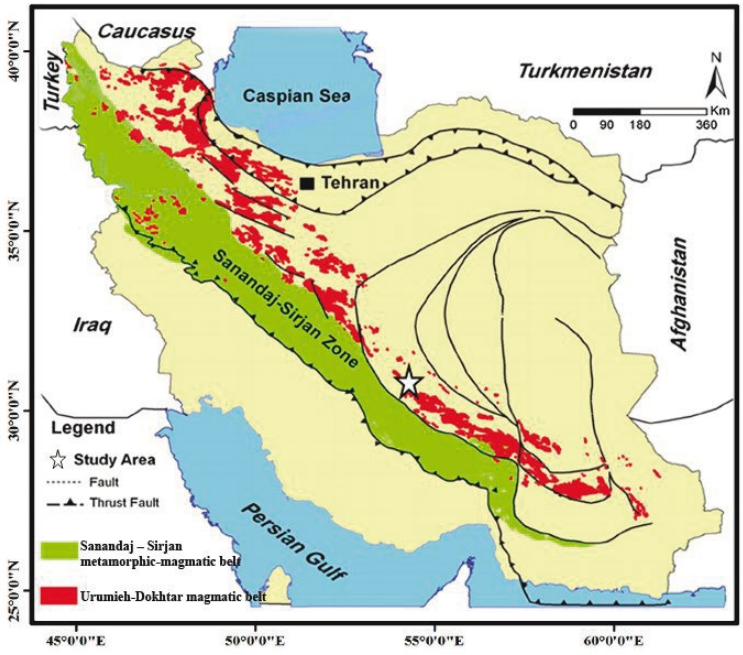

Figure 1. Location map of the study area along the Urmia-Dokhtar magmatic belt (modified from Alavi, 1994)

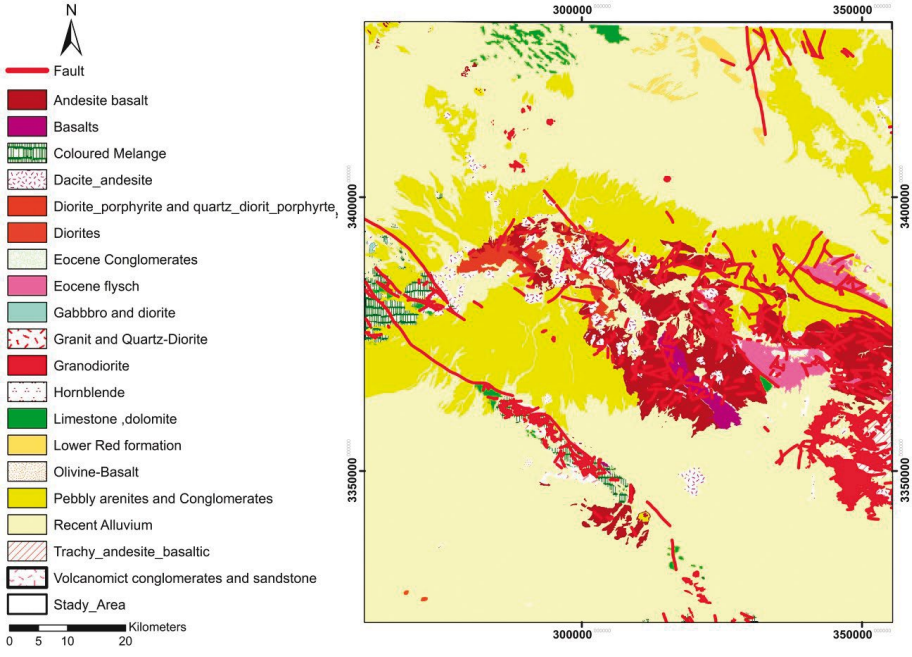

Figure 2. Simplified geologic map of the study area which is classified by age (modified from Soheili, 1981)

3. Materials and methods

There are a total of 31 porphyry Cu deposits distributed in the area (Table 1). Here, we applied fry, fractal, and distance-distribution analyses in a row to achieve the objectives of our study.

3.1. Fry analysis

As a visual tool for understanding the distribution of mineral deposits, fry analysis considers mineral deposits as points (Vearncombe and Vearncombe, 1999; Hassan Nezhad *et al*., 2001; Najafi *et al*., 2010; Zuo, 2015; Parsa *et al*., 2016b) to represent their spatial distribution (e.g., Kreuzer *et al*., 2007; Carranza, 2009; Parsa *et al*., 2018a). The method has been thoroughly described by Carranza (2009).

Fry analysis is a geometrical method for evaluating conformity of a geological point structure. It has been used by many geologists to analyse geological controllers of deposits (Kreuzer, *et al*., 2007 – Zuo, *et al*., 2009 – Carranza, 2009). It works by a transparent paper with horizontal and vertical axes intersecting at the centre of the paper. The centre point, marked by a sign, is superimposed on the corresponding point to a particular deposit and locations of other points are marked on the paper. The process is iterated for all points. Overall, the method leads to a total of n^2-n fry points, or the so-called translated points, from the analysis of n mineral deposit locations. The translated points are then demonstrated on rose diagrams manifesting the directions through which deposits are distributed. The rose diagrams are developed using the length and trend of the obtained points (Carranza, 2009). Dominant trends on the rose diagram demonstrate the trend of probable mineralization controllers, which needs to be confirmed with the help of local structural geology of the area, deposit type, and geological conditions of the deposits (Haddad- Martim *et al*., 2017). The rose diagrams can be produced in two different ways, namely using all points or a given set of them. If the former is the case, the rose diagram will serve as a visual aid for interpreting regional-scale distribution of mineral deposits. In contrast, the latter case shows the distribution of mineral deposits on a larger scale, depending on the selected intervals (Carranza, 2009; Haddad-Martim *et al*., 2017). Interested readers are referred to Carranza (2009) for further discussion.

The processes can be easily implemented using relevant software tools such as Geo Fry Plot, given probable linear trends as output.

3.2. Fractal analysis

Fractal measures have been frequently applied in different branches of earth sciences (e.g., Afzal *et al*., 2011; Mansouri *et al*., 2015; Yousefi *et al*., 2015; Yousefi *et al*., 2016; Parsa *et al*., 2017a; Parsa *et al*., 2017d), especially for understanding the subtle patterns embedded in the spatial distribution of mineral deposits (e.g., Carlson, 1991; Raines, 2008; Carranza, 2008; Carranza, 2009; Carranza and Sadeghi, 2014). Among a whole host of fractal measures proposed, the s-called box-counting (Pruess, 1995) and radial-density (Mandelbort, 1983) approaches can be used to assess spatial distribution of deposits, on which we will elaborate here.

3.2.1. Box-counting (B-C) measure

Fractal dimension of mineral deposits can be determined by the box-counting (B-C) method. In this method, a sheet is divided into a mesh of square cells of the size ε, and the cells with known mineralization points $N(\varepsilon)$ are counted. In order for the distribution pattern of the counted points to follow the fractal geometry, the conditions of the below power-law function have to be satisfied (Mandelbort, 1983; Feder, 1988; Pruess, 1995; Carranza, 2008; Carranza, 2009; Carranza and Sadeghi, 2014).

$$N(\varepsilon) \propto \varepsilon^{(-\beta)} \tag{1}$$

In the above equation, ∝ means proportion and β is the fractal dimension, which either ranges between 0 and 2, or is equal to 2. The latter case shows a complete spatial randomness. In a log-log plot, the equation will be a linear relationship, or (Carranza, 2008):

$$Log\,(N(\varepsilon)) = \alpha - \beta \,.\, Log(\varepsilon) \tag{2}$$

Where a is the intercept and β is the slope of the linear log–log plots of N (ε) versus ε.

3.2.2. Radial-density (*R-D*) measure

The Radial- Density (*R-D*) measure of fractality is expressed by the below equation (Mandelbrot, 1983):

$$d = C * r^{(D-2)} \tag{3}$$

In which d is the point density within a given location, C is a constant, r is the circle radius, and D is the fractal dimension. The foregoing function means that spatial distribution of points around a reference point is fractal should the point density decreases with distance from the reference point (Haddad-Martim *et al*., 2017). Actually, this method calculates the deposit density (i.e., the number of deposits / unit circle area) from a reference point. Interested readers are referred to Agterberg (2013) for further discussion.

3.3. Distance-distribution analysis

This method is perhaps the most popular method for measuring the spatial association of mineral deposits with geological structures (Berman, 1977, Berman, 1978 Berman, 1986) in a quantitative way (Carranza, 2008). Details about this method have been extensively explained by Carranza (2009), precluding us from further explanation. It works on the basis of three curves, namely, D_1, D_2, and the contrast curve (i.e., $C = D_2 - D_1$) measures the distance from each point to deposit locations, manifesting a complete spatial randomness. D_2, however, measures the distance of each structure from different deposit locations. Positive and negative values of C show positive and negative spatial associations of structures with mineralization, respectively (Carranza, 2008).

4. Results

Since Eocene, joints of the region have been among the oldest geological features and significantly contributed to forming regional faults. Joints play a crucial role in providing dikes with the required space for intrusion. Formation and concertation of joints into regional intrusive bodies have been affected by shearing mechanisms, geothermal solution pressure, and intrusive process of rock mass emplacement.

In order to determine the relationship between Cu mineralization and geological structures, data of faults and deposits across the study area was drawn (Fig. 3) and subjected to independent fractal analysis.

Table1. Locations of indices and Cu deposits in the study area (to be continued).

Main ore minerals	Alteration types	Host rocks	Y (D D)	X (D D)	Name	
Chalcopyrite, Chalcocite Covellite, Pyrite	Phyllic, Argillic, Propylitic, Silicification	Diorite porphyry, Quartz diorite porphyry	54.99	30.5	Abadia bagh	1
Pyrite, Chalcopyrite	Phyllic, Argillic, Propylitic, Potassic	Diorite porphyry	55.30	30.32	Abdar2	2
Pyrite, Chalcopyrite	Phyllic, Argillic, Propylitic, Silicification	Diorite porphyry Granodiorite porphyry,Andesite,	55.32	30.30	Abdar 1	3
Pyrite, Chalcopyrite	Phyllic, Argillic, Propylitic, Silicification	Diorite porphyry Granodiorite porphyry,Andesite,	54.94	30.52	Abdar chozam	4
Pyrite, Chalcopyrite	Phyllic, Argillic, Propylitic, Silicification	Diorite porphyry, Granodiorite porphyry,Andesite,	55.23	30.31	Adibagh	5
Pyrite,Chalcopyrite	Phyllic, Argillic, Propylitic, Silicification	Diorite porphyry, Granodiorite porphyry, Andesite	55.13	30.49	Bido	6
Pyrite, Chalcopyrite, Chalcocite	Phyllic, Argillic, Potassic, Propylitic, Jarositization	Diorite porphyry, Quartz diorite porphyry	55.17	30.41	Chah mesi 1	7
Pyrite, Chalcopyrite, Chalcocite	Phyllic, Argillic, Potassic Propylitic, Jarositization	Diorite porphyry, Quartz diorite porphyry	55.02	30.4	Chah firoozeh	8
Pyrite, Chalcopyrite	Phyllic, Argillic, Propylitic, Potassic	Diorite porphyry, Quartz diorite porphyry, Andesite	55.27	30.41	E E meydok	9
Pyrite, Chalcopyrite	Phyllic, Argillic, Propylitic, Potassic	Diorite porphyry	54.92	30.51	Eijo1	10
Pyrite, Chalcopyrite, Chalcocite, Malachite	Phyllic, Argillic, Propylitic, Potassic	Diorite porphyry	54.96	30.56	Eijo 2	11
Malachite, Azurite, Chrysocolla, Pyrite, Chalcopyrite	Phyllic, Propylitic, Potassic	Granodiorite porphyry	55.05	30.50	God kol vari 1	12
Pyrite, Chalcopyrite	Phyllic, Argillic, Propylitic, Potassic	Diorite porphyry, Quartz diorite porphyry, Andesite	54.97	30.61	God kol vari 2	13
Pyrite, Chalcopyrite	Phyllic, Argillic, Propylitic, Potassic	Diorite porphyry, Quartz diorite porphyry ,Andesite	55.01	30.61	God kol vari 3	14
Pyrite, Chalcopyrite	Phyllic, Argillic, Propylitic, Potassic	Diorite porphyry	54.99	30.59	God kol vari4	15
Malachite, Azurite, Chrysocolla, Pyrite, Chalcopyrite	Phyllic, Argillic, Potassic, Propylitic, Jarositization, Silicification	Diorite porphyry, Micro diorite porphyry	54.95	30.55	Eijo3	16
Pyrite,Chalcopyrite Chalcocite, Malachite,	Phyllic, Argillic, Propylitic, Potassic	Diorite porphyry	54.74	30.61	Kohe modavvar	18
Pyrite, Chalcopyrite, Galena	Phyllic, Argillic, Propylitic	Granodiorite porphyry, Dacite, Andesite, Diorite	55.19	30.38	Kohe mozahem	19

(*Continued*)

Table1. Locations of indices and Cu deposits in the study area

Main ore minerals	Alteration types	Host rocks	Y (D D)	X (D D)	Name	
Pyrite, Chalcopyrite	Phyllic, Argillic, Propylitic,	Granodiorite porphyry, Dacite, Andesite, Diorite	55.16	30.40	Lachah 1	20
Chalcopyrite, Malachite, Azurite	Carbonatization, Silicification, Propylitic, Chloritization, Sericitization,	Andesite, pyroclastites	55.16	30.41	Meydok	21
Chalcopyrite, Chalcocite, Sphalerite, Malachite, Azurite, Galena	Propylitic, Potassic	Andesite, Diorite porphyry	54.74	30.54	Nahro	22
Pyrite, Chalcopyrite	Phyllic, Argillic, Propylitic, Potassic	Diorite porphyry	54.90	30.27	Namakzar 1	23
Malachite, Azurite, Chrysocolla, Pyrite, Chalcopyrite	Phyllic, Argillic, Propylitic, Potassic	Diorite porphyry	54.81	30.37	Namakzar 2	24
Pyrite, Chalcopyrite	Phyllic, Argillic, Propylitic	Diorite porphyry, Quartz diorite porphyry ,Andesite	55.13	30.44	Parkam	25
Malachite, Azurite, Chrysocolla, Pyrite, Chalcopyrite	Phyllic, Argillic, Propylitic	Diorite porphyry	55.13	30.44	Sara	26
Malachite, Azurite, Chrysocolla, Pyrite, Chalcopyrite	Phyllic, Argillic, Propylitic	Diorite porphyry	54.99	30.48	Serenu	27
Malachite, Azurite, Chrysocolla, Pyrite, Chalcopyrite	Phyllic, Argillic, Propylitic, Potassic	Diorite porphyry	55.06	30.57	Tazarj	28
Pyrite, Chalcopyrite	Phyllic, Argillic, Propylitic, Silicification	Diorite porphyry, Granodiorite porphyry, Andesite	55.08	30.49	Tir koh	29
Chalcopyrite, Malachite, Azurite	Carbonatization, Silicification, Propylitic, Chloritization, Sericitization,	Andesite, pyroclastites	55.09	30.40	W E meydok	30
Pyrite, Chalcopyrite	Phyllic, Argillic, Propylitic	Diorite porphyry, Quartz diorite porphyry ,Andesite	54.98	30.47	Zavie olya	31

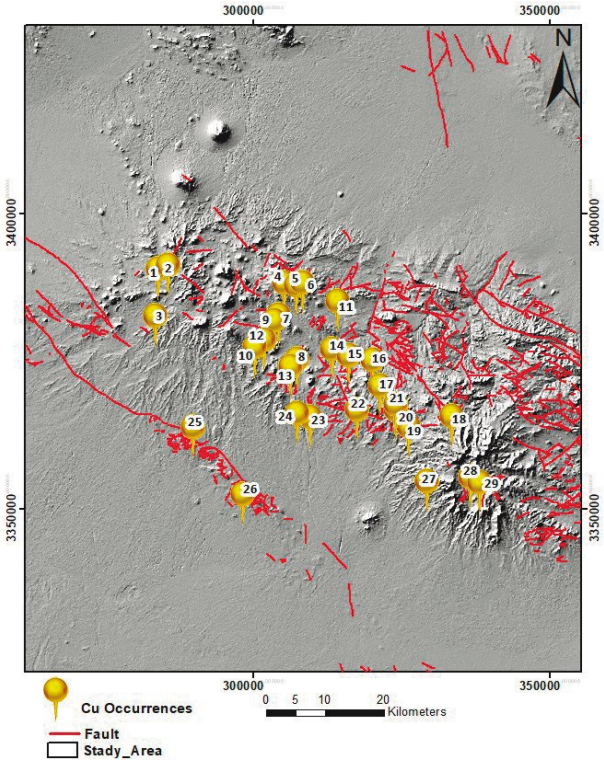

Figure 3. Location map of faults and deposits across the study area

4.1. Fractal analysis of faults

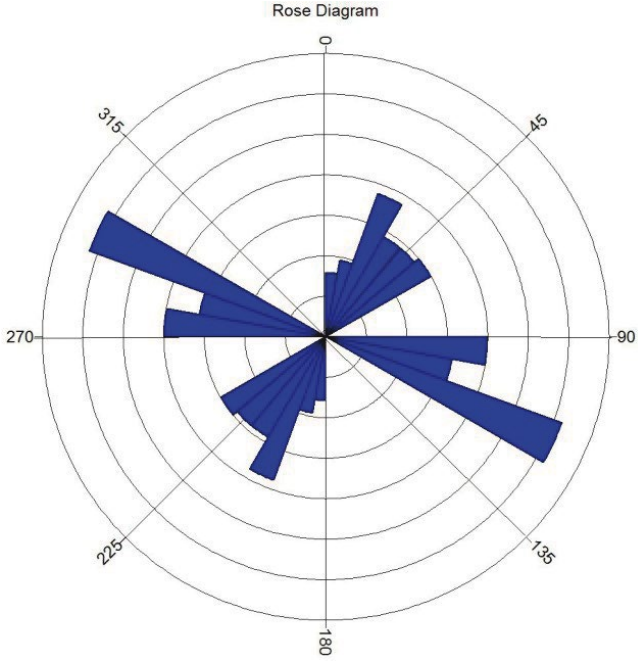

Figure 4. The rose diagram showing the distribution of faults in terms of length and direction

Acting as controlling factors to orebodies, patterns of local and regional fractures and geology of the area are of paramount importance. Satellite images enable geologists to identify associations between orebodies and regional lineaments. In a mineralization zone, the frequency of fractures and lineaments can lead exploration activities as they serve as channels for fluid flow.

Lineaments and fractures in a mineral zone may not be easily identifiable from satellite images. Accordingly, filtering is used to detect these features on the satellite images. The most popular kernels for feature detection are 3 * 3, 5 * 5, and 7 * 7 kernels. Knowing that the band 8 of the ETM^+ sensor provides for a higher spatial resolution than the other bands of the same sensor, we herein used band-8 data to detect lineaments, followed by applying three oriented filters at 0^0, 45^0, and 315° with a 3 * 3 kernel to identify regional fractures along N-S, NE-SW, and NW-SE directions, respectively.

Once finished with extracting the faults and fractures by means of the mentioned methodologies and correlating them to the fractures indicated on 1:100,000 map of the region, a new map of fractures was prepared. Afterwards rose diagrams of fractures and faults were plotted. The map of spatial distribution of faults, determined by the analysis of remotely sensed data, shows three major NE-SW, NS, and NW-SE- trending fault systems (Fig. 4). While NW-trending faults run parallel to magmatism in the area, NE-trending faults, that are younger than the first group (Mirzababaei, 2016; Zarasvandi *et al*., 2016), intersect with older geological units. The NS-trending faults, however, are apparently the youngest reportedly active faults on a local scale (Meshkani *et al*., 2013).

To determine fractal dimension of the faults, first, fracture maps of the area were divided into 4 squares grids of 48 km in side length (grids a, b, c, and d), with each grid sub divided into four identical squares. This process was iterated 6 times to come up with different numbers of squares and square sizes r at each iteration. Then, each square was analysed separately and a fractal dimension was calculated for each square grid (a, b, c, and d) (Fig. 5). Figure 5 shows a stepwise presentation of the box-counting method for measuring the fault fractal dimension (D). At each stage, the cells with the size r containing faults were counted and considered as $N(r)$ in Equations 1 and 2 (Table 2). On the basis of the logarithmic graphs plotted (Fig. 6), four fractal dimensions were calculated for the four grids a, b, c, and d (Fig. 6). The calculated values are D_a = 1.4339, D_b = 1.4971, $\boldsymbol{D_c = 1.5528}$, and D_d = 1.2777.

Table 2. Square dimension (r) and the number of cells containing faults (N) for 4 square grids a, b, c and d.

Level	r (km)	Box Count (N_a)	Box Count (N_b)	Box Count (N_c)	Box Count (N_d)
1	48	1	1	1	1
2	24	3	4	4	3
3	12	8	12	13	7
4	6	23	31	35	19
5	3	61	88	110	38
6	1.5	150	205	260	84

According to the results, the square grid c exhibits the largest fractal dimension, implying that it hosts the largest number of intersecting faults and hence, making it the most favourable part of the study area for prospecting further porphyry Cu deposits (cf. Carranza, 2009). Interestingly, deposits are more frequent in this region, showing the efficacy of the fractal method adopted. In other regions, however, the fractal dimension declines as they host fewer faults.

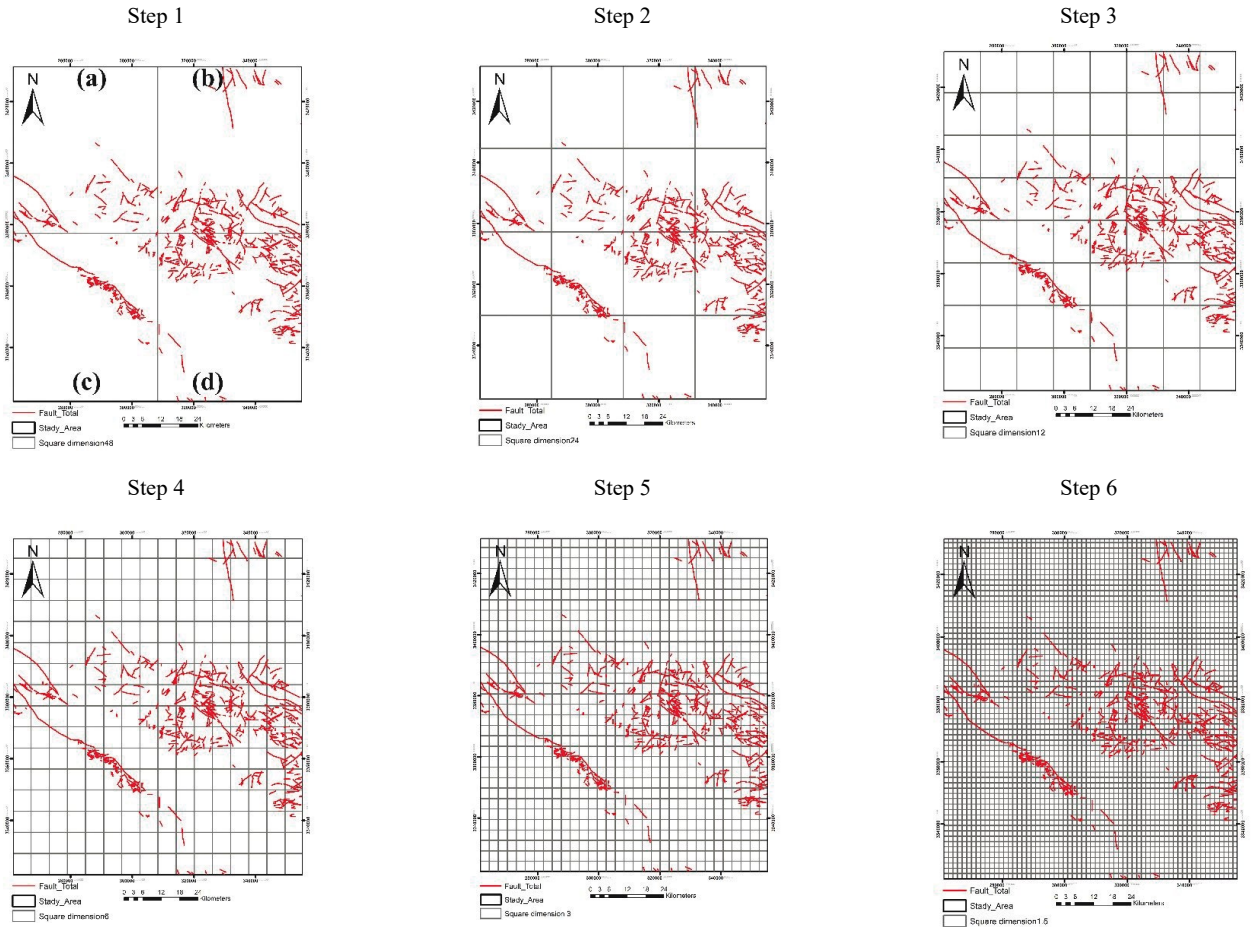

Figure 5. Stepwise presentation of the box-counting method.

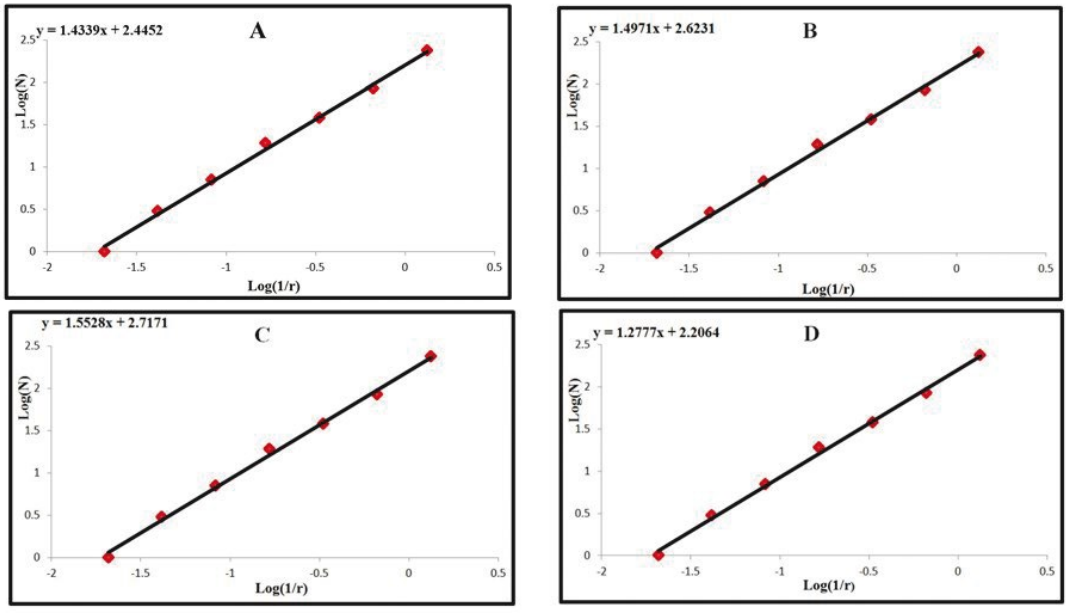

Figure 6. Log - log plot of the number of cells containing faults N(r) versus inverse of side length for square grids a, b, c, and d.

4.2. Fractal analysis for deposits

In order to implement the box-counting procedure, the study area was divided into a grid of cells with different dimensions in several steps and those that were superimposed by the deposits were counted. The log-log plot of the number of cells containing deposits $N(\varepsilon)$ versus the square length was prepared (Fig. 7). The *B-C* analysis exhibits that the pattern of the Cu deposits has two fractal dimensions, i.e., $\beta = (D_1 = 0.74$, and $D_2 = 0.85)$ and determined by one breakpoint on the plot (≈ 6 km).

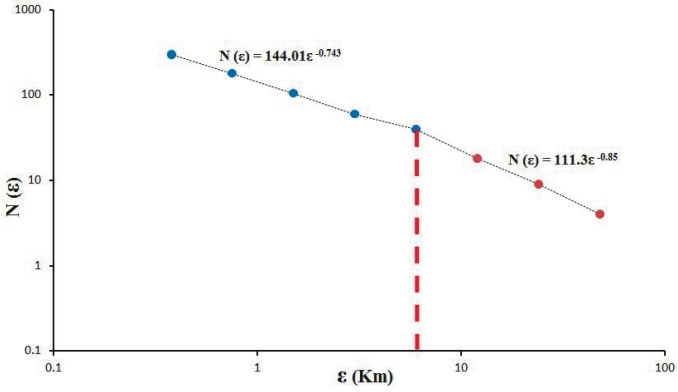

Figure 7. Log-log plot of the box–counting method showing N (ε) versus ε for the deposits

Authors also used the R-D fractal modelling (Fig. 8) to further investigate spatial distribution of the porphyry Cu deposits in Dehaj Area. For this purpose, the r-radius circles hosting Cu occurrences were counted. The result was, then divided by the area to obtain *d* in Equation 3 (Table 3). Figure 9 shows the log-log plot of radius (*r*) versus the density *(d*). As it can be observed in this figure, two fractal dimensions were observed, which were separated at around 6 km.

Table 3. Radius (*r*) and density (*d* = number of Cu occurrences in the circle/circle area).

Level	r (km)	number of Cu occurrences
1	48	31
2	24	23
3	12	17
4	6	6
5	3	1
6	1.5	0

Results of the two fractal methods (B-C, R-D) are almost identical, showing that two structural processes at different scales (< 6 km and > 6 km from the deposit locations) have controlled the emplacement of porphyry Cu deposits in Dehaj Area (Figs. 7 and 9).

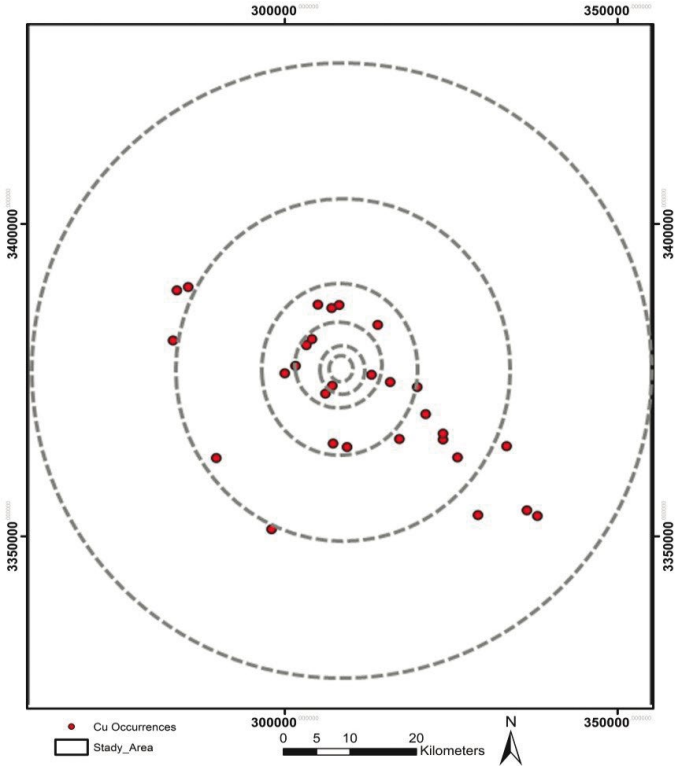

Figure 8. Stepwise presentation of the R–D method

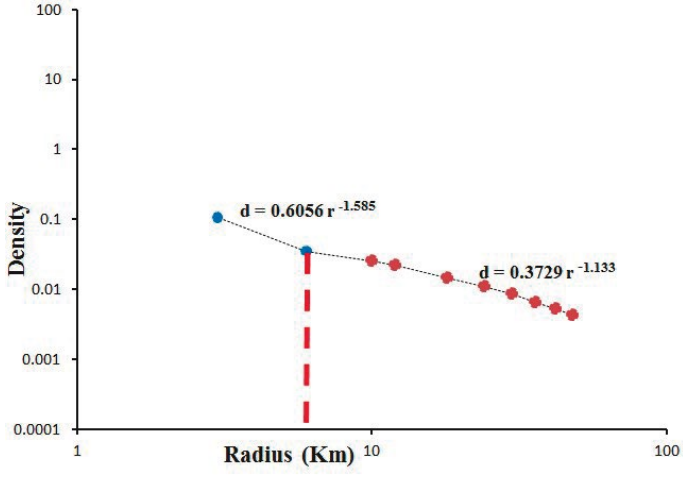

Figure 9. Log-log plot of the R–D method demonstrating radius (*r*) versus density (*d*) for deposits

4.3. Fry analysis for deposits

The fry analysis was applied on the 31 known porphyry Cu deposits in Dehaj Area, resulting in 930 fry points (Fig. 10). Initially, we used a rose diagram to show the trends of all fry points (Fig. 11a). This method sheds lights on the structural controls on mineralization that have acted on a regional scale (e.g., Parsa *et al*., 2018a). According to Fig. 10a, the regional controls on mineralization have plausibly operated in a major NW-SE and a minor E-W direction. Furthermore, with reference to the breakpoints separating fractal dimensions in Figs. 6 and 9, which are 6 km apart, we further developed a rose diagram for fry points that are within 6 km of one another (Fig. 11b). This figure shows a general N-S inclination, manifesting that local-scale controls on mineralization have probably contributed to the development of mineralization in an N-S direction.

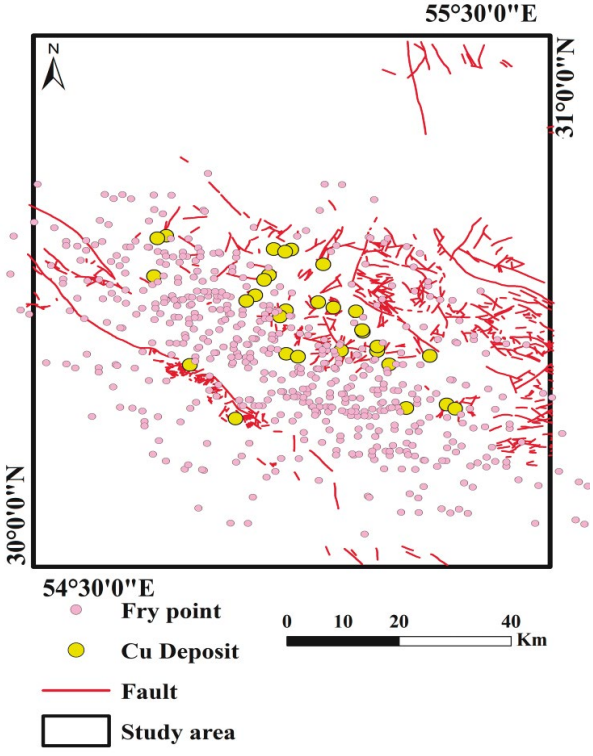

Figure 10. Points corresponding to local indices and fry

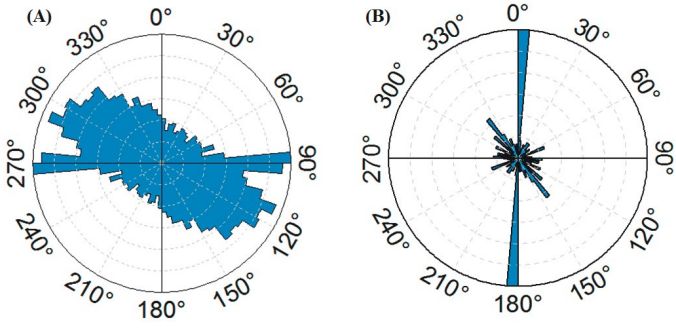

Figure 11. The rose diagram of (a) all fry analytical points, (b) points within 6 km of one another

Local investigation of Cu indices shows that, for the most part, Cu mineralization has occurred within intersection of faults with the mentioned trends. The fry pattern of the region and rose diagram of Cu index orientations indicate a general NW-SE trend, which is in good agreement with the trend of dominant fractures in the region.

4.4. Distance-Distribution analysis

Various structures, including faults with diverse directions, are resulted from different tectonic processes; however, only a limited number of tectonic processes are associated with mineralization (Faulkner *et al*., 2010). Therefore, mineralization-related tectonic processes should be identified. One way for recognizing mineralization-related fault systems is through measuring their spatial association with mineral deposits by the distance-distribution analysis; a positive relationship manifests a mineralization-related fault system while a negative relationship shows fault systems that are not associated with mineralization (Carranza, 2008). In this study, three distances -distribution graphs were plotted for three fault systems in the area, NW-, NE-, and N-trending faults (Fig. 12). According to this figure, all of these three fault systems are associated with porphyry Cu mineralization, as indicated by their positive association with mineral deposit locations. The highest positive spatial association between the NE-trending faults and mineralization was seen for the deposits within 6 km of the faults (Fig. 12a). Likewise, the highest positive spatial association was observed within a distance of about 10 km from the NW-trending faults (Fig. 12b). However, the most significant spatial correlation between mineralization and the N-trending faults is observed within a distance of merely 4 km from these faults (Fig. 12c). This shows that the NW- and NE-trending fault systems have controlled the distribution of faults on a regional scale while the N-trending faults have controlled the distribution of faults on a local scale.

5. Discussion

Porphyry Cu deposits are structurally controlled (Sillitoe, 1972, 2010; Padilla *et al*., 2001). Therefore, recognition of structural controls of this type of deposits is very important in exploration surveys. Analyses of spatial distribution of mineral deposits and spatial association of mineral deposits with fault systems can pave the way for addressing this challenge (Vearncombe and Vearncombe, 1999; Kreuzer *et al*., 2007; Lisitsin, 2015).

In order to investigate the regional fractures, an analysis was performed on the faults (including continuous and discontinuous faults) and the joints systems. Regional faults are dominantly strike-slip in nature (accompanied with small thrust or graben components in some cases) and follow different trends. Investigations showed that the regional faults have been formed as a result of the shearing effect applied to the Urmia-Dokhtar magmatic belt. Upon continuing the shearing mechanism and the resultant progressive deformation, alterations occurred to the faults and their geometrical associations. Regional joints systems are also developed as a result of the shearing mechanism and/or folding process. The progressive deformation within the shear zone has further affected the joints systems. A large number of jointed tuff strata have been rotated, with the other intrusive tuff bodies further experiencing shearing-induced changes. Another factor contributing to deformation of the region is the small shearing zones developed between the regional faults. Such shearing zones tend to further complicate the joints systems, mix up the strata, etc. Since the study area is located on the Urmia – Dokhtar igneous belt within the dextral shearing zone delimited by Rafsanjan Fault in the north and Shahr-e-Bakak Fault in the south (both of which are dextral strike-slip faults with some dip-slip components), then reginal fault analysis was performed on the basis of shearing mechanism. Existing literature have shown that NW-SE faults are the oldest in the region. For most part, these faults are longer than the other faults in the region, being observed along the longitudinal axis of intrusive bodies. Due to erosion and lack of visible evidence of the fault surface to ensure reactivation

of these faults, they seem to be primary faults in the region, which are formed sometime after the Eocene. If the amount of fault gouge along the fault surface is zero or negligible, the fault is said to be a periodic fault. This feature is seen for most of the faults in the region. Another characteristic of the faults in the region is the absence of fractures on the fault surface, which is another indication of faulted joints. Dominant trend of joints in the region is well in agreement with the trend of adjacent faults. Last but not the least, in-fills of chlorite and calcite can be seen on the fault surfaces for most of the faults in the region. The fact that the lithology of these in-fills is identical to that of near-fault periods further confirms that the mentioned faults are faulted joints.

The fractal analysis of the fault systems (e.g., Zhao *et al*., 2011), showed that the faults are significantly associated with mineralization (Figs. 5 and 6). In other words, an abundance of mineral deposits and fault systems is observable in the SE part of the area (grid C in Fig. 6) in which the fractal dimension is at its peak (1.748). These results are significant as fault systems are corridors for raising magmatic and hydrothermal fluids that develop mineralization (Pirajno, 2012).

Results of fry analysis (Fig. 11), fractal analysis (Figs. 7-9), and distance-distribution analysis (Fig. 12) were in agreement with one another showing that the NW- and NE- trending faults were responsible for regional-scale processes that have contributed to the development of mineralization. Furthermore, these analyses demonstrated that the N-trending faults are the local-scale controls on mineralization. These results have been achieved by numerical techniques in this paper and comply with the previous results achieved by other studies in Dehaj Area (Meshkani *et al*., 2013; Zarasvandi *et al*., 2016). In these studies, it has been reported that the NW-trending Dehshir-Baft strike-slip fault is the major structural control on the magmatism and the development of porphyry Cu deposits in the study area.

6. Conclusion

In this study, a range of numerical techniques were applied, including fry, fractal, and distance–distribution analyses, for the recognition of structural controls on porphyry Cu mineralization in Dehaj Area. By combining these methods, useful results were obtained to help understand the processes contributing to the formation of mineral deposits. Indeed, porphyry Cu masses were found to be more probable to intrude and accumulate along the margins of huge faults and shear zones. It was further indicated that evaluation of mineralization direction with respect to fault direction can provide insights into the role of faults in emplacement of Cu mineralization. Based on the results of spatial analysis, mineralization direction was conformed to faults directions in most parts of the study area. The fry analysis demonstrated that the study area had three intersecting fault mechanisms.

Fractal analysis of the fault systems revealed that the fractal dimension reaches its peak in the SE part of the area where there is an abundance of faults and mineral deposits, showing that faults are inextricably linked with porphyry Cu mineralization. In addition, the results of fry, fractal, and distance–distribution analyses of mineral deposit locations were in agreement with findings of previous geological studies of the area. These techniques demonstrated that whilst the NW- and NE-trending faults are responsible for the regional-scale deposition of mineralization in the area, the N-trending faults have probably acted as the local-scale controllers of mineralization in the area.

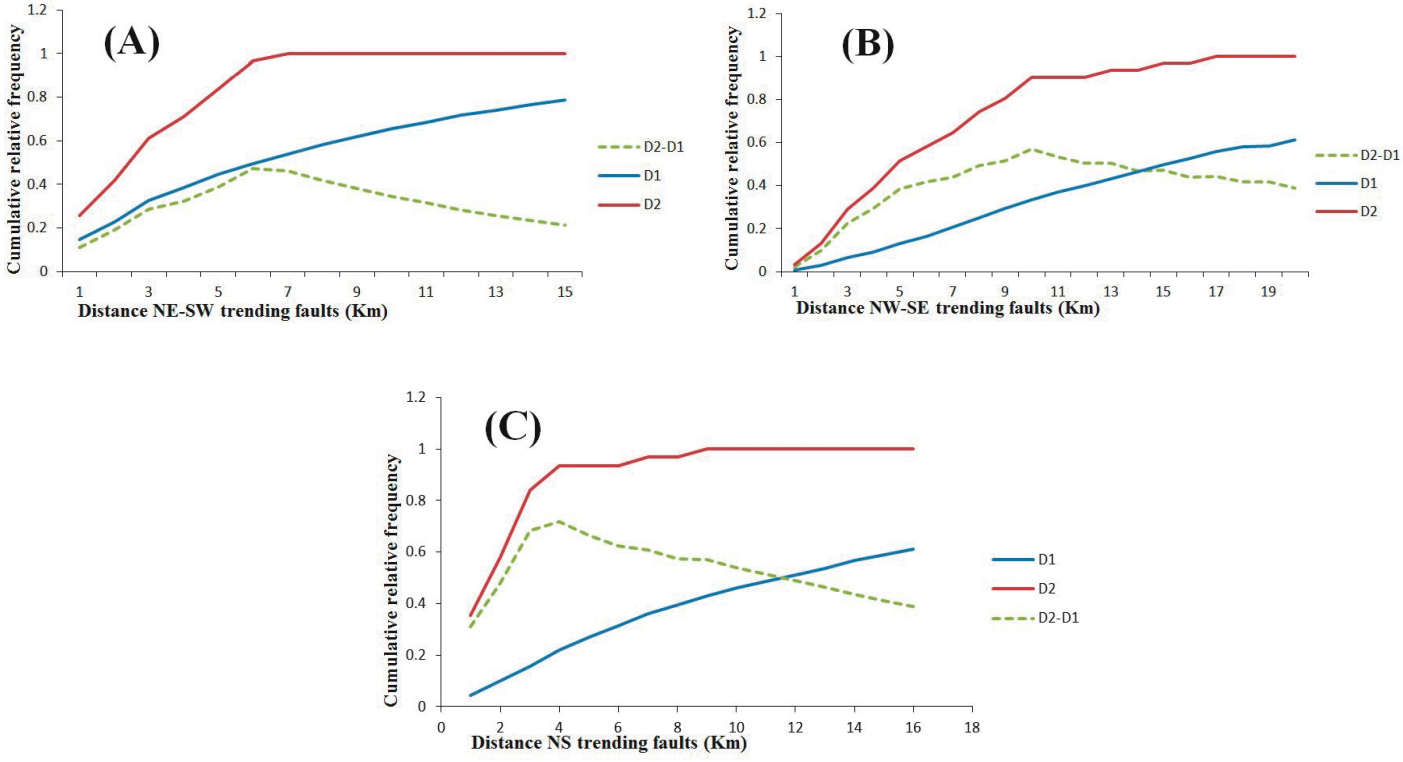

Figure 12. Distance-distribution analysis results to investigate the spatial relationship between fault systems and known deposits in the study area: (a) NE-trending faults (b) NW-trending faults and, (C) NS-trending faults.

References

Adib, A., Afzal, P., Mirzaei Ilani, S., & Aliyari, F. (2017a). Determination of the relationship between major fault and zinc mineralization using fractal modeling in the Behabad fault zone, central Iran. Journal of African Earth Sciences, 134, 308-319. https://doi.org/10.1016/j.jafrearsci.2017.06.025

Adib, A., Ilani, M. S., Shoaei, G. R. & Afzal, P. (2017b). Determination of a conceptual model for the structural features and Pb-Zn mineralization in the north of the Behabad fault zone, Central Iran. Iranian Journal of Earth Science, b9, 150-165.

Afzal, P., Alghalandis, Y. F., Khakzad, A., Moarefvand, P., & Omran, N. R. (2011). Delineation of mineralization zones in porphyry Cu deposits by fractal concentration–volume modeling. Journal of Geochemical Exploration, 108(3), 220-232. https://doi.org/10.1016/j.gexplo.2011.03.005

Agterberg, F. P. & Bonham-Carter, G. F. (2005). Measuring the performance of mineral potential maps. Journal of Natural Resources Research, 14, 1-17. https://doi.org/10.1007/s11053-005-4674-0

Agterberg, F. P. (2013). Fractals and spatial statistics of point patterns. Journal of Earth Science, 24, 1–11. https://doi.org/10.1007/s12583-013-0305-6

Alavi, M. (1994). Tectonics of the Zagros orogenic belt of Iran: new data and interpretations. Tectonophysics, 229(3-4), 211-238. https://doi.org/10.1016/0040-1951(94)90030-2

Bazin, D. & Hubner, H. (1969). Copper deposits in Iran. Geological survey of Iran, Tehran, 232 pp.

Berman, M. (1977). Distance distributions associated with Poisson processes of geometric figures. Journal of Applied Probability, 14, 195–199. https://doi.org/10.2307/3213273

Berman, M. (1986). Testing for spatial association between a point process and another stochastic process. Journal of Applied Statistics, 35, 54-62. https://doi.org/10.2307/2347865

Carlson, C. A. (1991). Spatial distribution of ore deposits. Journal of Geology, 19(2), 111-114. https://doi.org/10.1130/0091-7613(1991)019<0111:SDOOD>2.3.CO;2

Carranza, E. J. M. (2008). Geochemical Anomaly and Mineral Prospectivity Mapping in GIS. Elsevier B.V, Amsterdam, Netherlands, 351 pp.

Carranza, E. J. M. (2009). Controls on mineral deposit occurrence inferred from analysis of their spatial pattern and spatial association with geological features. Ore Geology Reviews, 35(3-4), 383-400. https://doi.org/10.1016/j.oregeorev.2009.01.001

Carranza, E. J. M. & Sadeghi, M. (2014). Post-VMS mineralization deformations (1880–1820 Ma) of the Skellefte district (Sweden): insights from the spatial pattern of VMS occurrences. Journal of Frontiers of Earth Science, 8, 319–324. https://doi.org/10.1007/s11707-014-0466-3

Dehghani, B. (2000). Petrological and geochemical study in Darreh–Zereshk and Turan Posht, Southwestern of Yazd. [Master's Thesis, Tehran University], Tehran, Iran.

Dimitrijevic, M. D. (1973). Geology of Kerman Region. Geological Survey of Iran, Tehran, Iran.

Faulkner, D., Jackson, C., Lunn, R., Schlische, R., Shipton, Z., Wibberley, C., & Withjack, M. (2010). A review of recent developments concerning the structure, mechanics and fluid flow properties of fault zones. Journal of Structural Geology, 32(11), 1557-1575. https://doi.org/10.1016/j.jsg.2010.06.009

Feder, J. (1988). Fractals. Plenum Press, New York, USA, 282 pp.

Feizi, F., KarbalaeiRamezanali, A. & Mansouri, E. (2017a). Calcic iron skarn prospectivity mapping based on fuzzy AHP method, a case Study in Varan area, Markazi province, Iran. Geosciences Journal, 21(1), 123-136. https://doi.org/10.1007/s12303-016-0042-9

Feizi, F., Karbalaei-Ramezanali, A. & Tusi, H. (2017b). Mineral potential mapping via TOPSIS with hybrid AHP–Shannon entropy weighting of evidence: a case study for porphyry-cu, Farmahin area, Markazi Province, Iran. Natural Resources Research, 26(4), 553-570. https://doi.org/10.1007/s11053-017-9338-3

Fry, N. (1979). Random point distributions and strain measurement in rocks. Tectonophysics, 60(1-2), 89-105. https://doi.org/10.1016/0040-1951(79)90135-5

Haddad-Martim, P. M., Souza Filho, C. R. D., & Carranza, E. J. M. (2017). Spatial analysis of mineral deposit distribution: A review of methods and implications for structural controls on iron oxide-copper-gold mineralization in Carajás, Brazil. Ore Geology Reviews, 81, 230-244. https://doi.org/10.1016/j.oregeorev.2016.09.038

Hassan Nezhad, A., Moore, F. & Aliabadi, M.A. (2001). Lineament controller of spatial distribution of copper deposits of Zn-Pb deposits in Iran, Using Fry analysis. 5th Symposium of Geological Society of Iran, Tehran University, Tehran, Iran.

Khakzad, A. & Jaafari, H. (2002). Mineralogy and economic geology of copper deposits of Harare district in Kerman province. 10th Symposium of Crystallography and Mineralogy, Tehran, Iran, August, 168-172.

Khoie, N., Ghorbani, M. & Tajbakhsh, P. (1999). Copper Deposits of Iran, Geological Survey of Iran (in Persian). Tehran, 421 pp.

Kreuzer, O., Blenkinsop, T., Morrison, R., & Peters, S. (2007). Ore controls in the Charters Towers goldfield, NE Australia: Constraints from geological, geophysical and numerical analyses. Ore Geology Reviews, 32(1-2), 37-80. https://doi.org/10.1016/j.oregeorev.2006.12.001

Lisitsin, V. (2015). Spatial data analysis of mineral deposit point patterns: Applications to exploration targeting. Ore Geology Reviews, 71, 861-881. https://doi.org/10.1016/j.oregeorev.2015.05.019

Mandelbrot, B. B. (1983). The Fractal geometry of nature. W. H. Freeman, San Francisco, CA, 14 pp.

Mansouri, E., Feizi, F., & Karbalaei Ramezanali, A. A. (2015). Identification of magnetic anomalies based on ground magnetic data analysis using multifractal modelling: a case study in Qoja-Kandi, East Azerbaijan Province, Iran. Nonlinear Processes in Geophysics, 22(5), 579-587. DOI: 10.5194/npgd-2-1137-2015

Mehrabi, A., Rangzan, K., & Zarasvandi, A., (2005). Where is significant location for the porphyry copper Deposits? A case study in south central Iranian volcanic belt. 9th symposium of Geological Society of Iran, The teacher Training University, Tehran, Iran.

Meshkani, S. A., Mehrabi, B., Yaghubpur, A., & Sadeghi, M. (2013). Recognition of the regional lineaments of Iran: Using geospatial data and their implications for exploration of metallic ore deposits. Ore Geology Reviews, 55, 48-63. https://doi.org/10.1016/j.oregeorev.2013.04.007

Mirzababaei, G., Shahabpour, J., Zarasvandi, A. M., & Hayatolghey, S. (2016). Structural Controls on Cu Metallogenesis in the Dehaj Area, Kerman Porphyry Copper Belt, Iran: A Remote Sensing Perspective. Journal of Sciences, Islamic Republic of Iran, 27(3), 253 – 267.

Najafi, A., Abdi, M., Rahimi, B., & Motevali, K. (2010). Spatial integration of fray and fractal analyses in regional exploration: A case study from Bafgh-Posht-e-Badam, Iran. Geología Colombiana, 35, 113-130.

Padilla Garza, R. A., Titley, S. R., & Francisco Pimentel, B. (2001). Geology of the Escondida porphyry copper deposit, Antofagasta region Chile. Economic Geology, 96(2), 307-344. https://doi.org/10.2113/gsecongeo.96.2.307

Parsa, M., Maghsoudi, A., Yousefi, M., & Sadeghi, M. (2016a). Prospectivity modeling of porphyry-Cu deposits by identification and integration of efficient mono-elemental geochemical signatures. Journal of African Earth Sciences, 114, 228-241. https://doi.org/10.1016/j.jafrearsci.2015.12.007

Parsa, M., Maghsoudi, A., Yousefi, M., & Sadeghi, M. (2016b). Recognition of significant multi-element geochemical signatures of porphyry Cu deposits in Noghdouz area, NW Iran. Journal of Geochemical Exploration, 165, 111-124. https://doi.org/10.1016/j.gexplo.2016.03.009

Parsa, M., Maghsoudi, A., Carranza, E. J. M., & Yousefi, M. (2017a). Enhancement and mapping of weak multivariate stream sediment geochemical anomalies in Ahar Area, NW Iran. Journal of Natural Resources Research, 26, 443-455. https://doi.org/10.1007/s11053-017-9346-3

Parsa, M., Maghsoudi, A., Yousefi, M., & Carranza, E. J. M. (2017b). Multifractal interpolation and spectrum–area fractal modeling of stream sediment geochemical data: Implications for mapping exploration targets. Journal of African Earth Sciences, 128, 5-15. https://doi.org/10.1016/j.jafrearsci.2016.11.021

Parsa, M., Maghsoudi, A., & Yousefi, M. (2017c). An improved data-driven fuzzy mineral prospectivity mapping procedure; cosine amplitude-based similarity approach to delineate exploration targets. International Journal of Applied Earth Observation and Geoinformation, 58, 157-167. https://doi.org/10.1016/j.jag.2017.02.006

Parsa, M., Maghsoudi, A., Yousefi, M., & Sadeghi, M. (2017d). Multifractal analysis of stream sediment geochemical data: Implications for hydrothermal nickel prospection in an arid terrain, eastern Iran. Journal of Geochemical Exploration, 181, 305-317. https://doi.org/10.1016/j.gexplo.2016.11.013

Parsa, M., Maghsoudi, A., & Yousefi, M. (2018a). Spatial analyses of exploration evidence data to model skarn-type copper prospectivity in the Varzaghan district, NW Iran. Ore Geology Reviews, 92, 97-112. https://doi.org/10.1016/j.oregeorev.2017.11.013

Parsa, M., Maghsoudi, A., & Yousefi, M. (2018b). A receiver operating characteristics-based geochemical data fusion technique for targeting undiscovered mineral deposits. Natural Resources Research, 27(1), 15-28. https://doi.org/10.1007/s11053-017-9351-6

Parsa, M., & Maghsoudi, A. (2018). Controls on Mississippi Valley-Type Zn-Pb mineralization in Behabad district, Central Iran: Constraints from spatial and numerical analyses. Journal of African Earth Sciences, 140, 189-198. https://doi.org/10.1016/j.jafrearsci.2018.01.012

Pirajno, F. (2012). Hydrothermal mineral deposits: principles and fundamental concepts for the exploration geologist. Springer-Verlag, Berlin 709pp.

Pruess, S. A. (1995). Some remarks on the numerical estimation of the fractal dimension. Journal of Fractals in the Earth Sciences, 00, 65-75. DOI: 10.1007/978-1-4899-1397-5_3

Raines, G. L. (2008). Are fractal dimensions of the spatial distribution of mineral deposits meaningful. Journal of Progress in Geomathematics, 285–301. https://doi.org/10.1007/s11053-008-9067-8

Ramezanali, A. K., Feizi, F., Jafarirad, A., & Lotfi, M. (2019). Geochemical Anomaly and Mineral Prospectivity Mapping for Vein-Type Copper Mineralization, Kuhsiah-e-Urmak Area, Iran: Application of Sequential Gaussian Simulation and Multivariate Regression Analysis. Natural Resources Research, 1-30. https://doi.org/10.1007/s11053-019-09565-7

Ryan, P. D. & Dewey, J. F. (1990). A geological and tectonic cross-section of the Caledonides of western Ireland. Journal of the Geological Society, 173-180. https://doi.org/10.1144/gsjgs.148.1.0173

Sillitoe, R. H. (1972). A plate tectonic model for the origin of porphyry copper deposits. Economic Geology, 67, 184-197. https://doi.org/10.2113/gsecongeo.67.2.184

Sillitoe, R. H. (2010). Porphyry copper systems. Economic Geology, 105, 3-41. https://doi.org/10.2113/gsecongeo.105.1.3

Soheili, M. (1981). Geological Quadrangle Map of Iran (1:250000 Series sheet) NO. H- 10.

Tanhaei, N., Hassan Nezhad, A., & Dabestani, N. (2010). Lineament controller of spatial distribution of copper deposits of copper deposits in Iran, Using Fry analysis. Initial symposium of Iranian Society of Economic Geology. Ferdowsi University of Mashhad, Mashhad, Iran.

Vearncombe, J., & Vearncombe, S. (1999). The spatial distribution of mineralization: applications of fry analysis. Journal of Economic Geology, 94(4), 475-486. https://doi.org/10.2113/gsecongeo.94.4.475

Walker, R. T. (2006). A remote sensing study of active folding and faulting in southern Kerman province, S.E. Iran. Journal of Structural Geology, 28(4), 654-668. https://doi.org/10.1016/j.jsg.2005.12.014

Xiao, F., Chen, J., Zhang, Z., Wang, C., Wu, G., & Agterberg, F. P. (2012). Singularity mapping and spatially weighted principal component analysis to identify geochemical anomalies associated with Ag and Pb-Zn polymetallic mineralization in Northwest Zhejiang, China. Journal of Geochemical Exploration, 122, 90-100. https://doi.org/10.1016/j.gexplo.2012.04.010

Yaghoubpour, A., & Hassan Nezhad, A. A. (2006). The Spatial Distribution of Some Chromite Deposits in Iran, Using Fry Analysis. Journal of Sciences, Islamic Republic of Iran, 17(2), 147-152.

Yousefi, M., & Carranza, E. J. M. (2015). Prediction–area (P–A) plot and C–A fractal analysis to classify and evaluate evidential maps for mineral prospectivity modeling. Computers & Geosciences, 79, 69-81. https://doi.org/10.1016/j.cageo.2015.03.007

Yousefi, M., & Carranza, E. J. M. (2017). Union score and fuzzy logic mineral prospectivity mapping using discretized and continuous spatial evidence values. Journal of African Earth Sciences, 128, 47-60. https://doi.org/10.1016/j.jafrearsci.2016.04.019

Zarasvandi, A. (2004). Magmatic and structural controls on localization of the Darreh-Zerreshk and Ali-Abad porphyry copper deposits, Yazd Province, Central Iran. [Doctoral thesis, Shiraz University], Shiraz, Iran, 280 pp.

Zarasvandi, A., Pourkaseb, H., & Jalili, Y. (2016). Investigation on the relationship between copper mineralization in Khezr Abad and Shahrebabak area: regions: Using Fractal and fry analyzes. Journal of Economic Geology, 7(2), 385-402.

Zhao, J., Chen, S., Zuo, R., & Carranza, E. J. M. (2011). Mapping complexity of spatial distribution of faults using fractal and multifractal models: vectoring towards exploration targets. Computers & Geosciences, 37(12), 1958-1966. https://doi.org/10.1016/j.cageo.2011.04.007

Zuo, R., Agterberg, F. P., Cheng, Q., & Yao, L. (2009). Fractal characterization of the spatial distribution of geological point processes. International Journal of Applied Earth Observation and Geoinformation, 11(6), 394-402. https://doi.org/10.1016/j.jag.2009.07.001

Zuo, R., Wang, J., Chen, G., & Yang, M. (2015). Reprint of "Identification of weak anomalies: A multifractal perspective". Journal of Geochemical Exploration, 154, 200-212. https://doi.org/10.1016/j.gexplo.2015.04.004